九州大学学術情報リポジトリ
Kyushu University Institutional Repository

Recent Increases in Hippocampal Tau Pathology in the Aging Japanese Population: The Hisayama Study

濱﨑, 英臣

https://hdl.handle.net/2324/2236115

出版情報：Kyushu University, 2018, 博士（医学）, 課程博士
バージョン：
権利関係：

Recent increases in hippocampal tau pathology in the aging Japanese population: the Hisayama study

Hideomi Hamasaki[a], Hiroyuki Honda[a], Tsuyoshi Okamoto[b,c], Sachiko Koyama[a], Satoshi O. Suzuki[a], Tomoyuki Ohara[d,e], Toshiharu Ninomiya[e,f], Yutaka Kiyohara[g], and Toru Iwaki[a]

[a]Department of Neuropathology, Graduate School of Medical Sciences, Kyushu University, Fukuoka, Japan

[b]Faculty of Arts and Science, Kyushu University, Fukuoka, Japan

[c]Graduate School of Systems Life Sciences, Kyushu University, Fukuoka, Japan

[d]Department of Neuropsychiatry, Graduate School of Medical Sciences, Kyushu University, Fukuoka, Japan

[e]Department of Epidemiology and Public Health, Graduate School of Medical Sciences, Kyushu University, Fukuoka, Japan

[f]Department of Center for Cohort Studies, Graduate School of Medical Sciences, Kyushu University, Fukuoka, Japan

[g]Hisayama Research Institute for Lifestyle Diseases, Fukuoka, Japan

Running title: Recent trends in hippocampal tau pathology

*Corresponding author: Toru Iwaki, Department of Neuropathology, Graduate School of Medical Sciences, Kyushu University, 3-1-1 Maidashi, Higashi-ku, Fukuoka 812-8582, Japan.

Tel: +81-92-642-5536; Fax: +81-92-642-5540

E-mail: iwaki@np.med.kyushu-u.ac.jp.

Running title: Recent trends in hippocampal tau pathology

Abstract.

Background: The Hisayama study is a prospective cohort study of lifestyle-related diseases that commenced in 1961. Through it, a significant increasing trend in the prevalence of Alzheimer's disease has been observed over the past 18 years.

Objectives: We sought to investigate the increases in brain pathology related to Alzheimer's disease using automated MATLAB morphometric analyses for quantifying tau pathology.

Methods: We examined a series of autopsied cases from Hisayama residents obtained between 1998 and 2003 (group A: 203 cases), and between 2009 and 2014 (group B: 232 cases). We developed custom software in MATLAB to analyze abnormal tau deposits quantitatively. Specimens were immunostained with both anti-β-protein and anti-phosphorylated tau antibodies.

Results: Both the Consortium to Establish a Registry for Alzheimer's Disease (CERAD) criteria for senile plaques and Braak stage for NFT were higher in group B. Morphometric analyses of the hippocampi also revealed a trend towards increased tau pathology in both men and women over 80 years of age in group B. The increases were also significant when the subjects were examined independently according to high or low CERAD scores and in all levels of AD neuropathologic change according to the National Institute on Aging-Alzheimer's Association guidelines (2012).

Conclusion: We revealed a recent trend of increased tauopathy in the older people, which is partly independent of Aβ pathology.

Keywords: Alzheimer’s disease, tauopathy, neurofibrillary tangles, image analysis

INTRODUCTION

The World Alzheimer Report 2015 documented that dementia affects over 46 million people worldwide, and that this number is estimated to increase about 3-fold by 2050 [1]. In Japan, the population is becoming increasingly aged, so dementia has become a critical social problem. Alzheimer's disease (AD) is the most common cause of dementia and is known to be associated with lifestyle-related diseases such as abnormal lipid metabolism and insulin resistance [2, 3]. The deposition of hyperphosphorylated tau in brains, tauopathy, is implicated in a wide variety of neurodegenerative diseases, including AD. Tau deposits are characterized by their location and shape, in addition to the individual tau protein isoform involved. The two main pathological features of the AD brain are well known; the deposits of β-proteins, known as senile plaques, and the aggregation of hyperphosphorylated tau, known as neurofibrillary tangles (NFT).

The town of Hisayama, a suburb of Fukuoka, Japan, has demographic characteristics representative of the national average of Japan, including the distribution of age, occupational status, and nutrient intake [4]. In Hisayama, a long-term prospective cohort study of cerebro-cardiovascular diseases has been running since 1961. This population-based study has shown that the prevalence of all-cause dementia and AD significantly increased between 1985 and 2005 [5]. The Hisayama study has also revealed an association between lifestyle factors and

dementia [6-8]. The aim of the current study was to quantitatively assess the brain pathologies related to AD and to investigate the changes in pathology in an aged population.

MATERIALS AND METHODS

Subjects

This study included specimens from a series of autopsies performed on residents of the town of Hisayama in Fukuoka Prefecture, Japan. There were two groups, group A (1998–2003; 203 cases; mean age at death, 78.8 ± 12.8 years, range, 32–100 years) and group B (2009–2014; 232 cases; mean age at death, 83.0 ± 10.8 years, range, 42–105 years), with approximately 10 years difference between the survey dates of these groups. The characteristics of the two groups are shown in Table 1 and 2. The clinical diagnosis of dementia was made based on the Diagnostic and Statistical Manual of Mental Disorders, Third Edition – Revised [9]. Details of the clinical survey have been described in a previous report [5].

The study was approved by the Ethics Committee of the Faculty of Medicine, Kyushu University, and was performed in accordance with the ethical standards described in the fifth revision of the Declaration of Helsinki, 2000.

Neuropathological assessment

The brains were weighed and fixed in 10% buffered formalin for at least 2 weeks. The specimens included the middle frontal gyrus, superior and middle temporal gyri, inferior parietal lobule, hippocampus with entorhinal cortex and transentorhinal cortex (at the level of the lateral geniculate body), calcarine cortex, basal ganglia including the nucleus basalis of Meynert, thalamus, substantia nigra, locus ceruleus, and the dorsal vagal nucleus. Sections were embedded in paraffin and routinely stained using hematoxylin-eosin, the Klüver-Barrera, and a modified Bielschowsky method [10]. The specimens were immunostained using antibodies against the phosphorylated microtubule-associated protein tau (clone AT8, mouse monoclonal, 1:500; Innogenetics, Ghent, Belgium) and against β-protein (clone 6F/3D, mouse monoclonal, 1:200; Dako, Glostrup, Denmark) after antigen retrieval by autoclaving in 0.01 M citrate buffer, pH 8 or incubating in 90% formic acid in one hour, respectively, and detected using a standard indirect immunoperoxidase method and visualized using diaminobenzidine (Dojindo, Kumamoto, Japan) as a chromogen. Senile plaques were detected using both a modified Bielschowsky method and immunohistochemistry for β-protein (Aβ). The assessment of AD pathology was assessed according to the Consortium to Establish a Registry for Alzheimer's disease (CERAD) guidelines [11] and Braak and Braak stage [12, 13]. The CERAD score and

Braak and Braak stage were combined to estimate the likelihood of AD. The pathological diagnosis of AD was conducted according to the National Institute on Aging (NIA)-Reagan Institute criteria [14]. Additionally, we also subdivided all cases into four levels of AD neuropathologic change; “Not”, “Low”, “Intermediate”, or “High”, according to NIA-Alzheimer’s Association (NIA-AA) guidelines using a combination of Braak, CERAD and Thal scores [15]. The frequency of neuritic plaques was semiquantitatively categorized into the following four groups: none, sparse, moderate, and frequent according to CERAD criteria (Table 1). The severity of the NFTs was semiquantitatively categorized into six groups, stages I–VI, according to Braak and Braak stage criteria (Table 1). To evaluate the relationship between tau deposits and CERAD stage, we categorized the data into low CERAD score (none and sparse) and high CERAD score (moderate and frequent) groups. The neuropathological assessment of dementia with Lewy bodies (DLB) was performed using standard diagnostic criteria for DLB [16, 17]. The neuropathological changes of the 203 cases in group A were examined as described previously [5].

Image analyses using custom software in MATLAB

We developed custom software in MATLAB (MathWorks Inc., Natick, MA, USA) for

quantitatively analyzing abnormal tau deposits including NFTs and pre-tangles and other neuropil tau pathologies including neuropil threads, grains, and neuritic plaques (Figs. 1 and 2). From the results of the immunohistochemical analyses using AT8 we chose the most aberrant regions of tau deposits as the regions of interest (ROI) and captured images with a 20× objective lens with a total field size of 704 × 528 μm^2 and pixel numbers of 1600 × 1200 pixels (0.44 μm × 0.44 μm/pixel; Fig. 2A). The minimum size we calculated was 1 pixel: 0.44×0.44 μm^2. The color space of each image captured was converted from RGB to CIE 1976 L* (brightness) a* (green to magenta) b* (blue to yellow) color space using the MATLAB and the Euclidean distance in CIE 1976 L*a*b* color space was calculated. The CIE 1976 L*a*b* color is more suitable for quantifying human vision than the RGB color space. In CIE 1976 L*a*b*, the differences between any two colors can be approximated by taking the Euclidean distance between them [18]. More details of the conversion of RGB to CIE 1976 L*a*b* are available from MathWorks [19]. Abnormal tau deposits were then divided into three groups including the tau deposits, the backgrounds, and questionable or ambiguous staining, by K-means clustering [20]. After removing small objects of four or fewer pixels as noise, we calculated a variety of indices characterizing the extracted abnormal tau deposits in regards to morphology (e.g., circularity and eccentricity) and size (e.g., area, corresponding radius, and perimeter). The total

number of abnormal tau deposits was also calculated. We constructed a scatter plot of the circularity versus the relative corresponding radius and calculated Euclidean distances between each plot. We then automatically classified abnormal tau deposits into three groups including NFTs and other small-size tauopathies, with or without large circularity, by K-means clustering (Figs. 3B and E). The perimeter (L) and area (S) were calculated directly to give the polygon length and area. Circularity, a parameter of the shape complexity, was defined as:

$$Circularity = 4\pi S/L^2.$$

The corresponding radii were calculated as

$$Corresponding\ radii = \sqrt{(S/\pi)}.$$

Finally, we obtained the total number and the total area (μm^2) of tau deposits, NFTs, and neuropil tau deposits, and calculated the percentage of area per total field size. These indices can be used for quantitatively evaluating NFT and neuropil tau deposits.

Quantitative analyses of tau deposits in the cornu ammonis 1 (CA1) region

The CA1 area of the hippocampus is vulnerable to tauopathy, and abnormal tau deposits are noted in the region through from the initial to the most advanced stage of Braak and Braak staging. Therefore, we considered the CA1 area a very suitable region in which to elucidate

sequential tau pathology in human brains. We analyzed the CA1 region in 203 of the 209 autopsied cases in group A and 232 of the 235 autopsied cases in group B. Six cases in group A and three in group B were excluded from the digital analyses, because the brain specimens had severe damage (n = 6) or the brains of were not examined by autopsy (n = 3). The CA1 region with most intense tau deposits was chosen and imaged using a 20× objective lens. The images captured were quantitatively analyzed using our new programs to reveal areas, numbers, and morphometric indices including corresponding radius, circularity, and eccentricity.

Statistical analyses

Statistical analyses were conducted using JMP Pro 11 (SAS Institute, Cary, NC, USA). The p values of mean age at death were calculated by Welch's t test, and the p values of the median area of total tau deposits, NFTs, and neuropil tau deposits were calculated using Mann–Whitney U tests. Significance was defined as $p < 0.05$.

RESULTS

CERAD stage and Braak and Braak stage trends

Compared with group A, both the CERAD stage for senile plaques and Braak and Braak stage

for NFT were higher in group B (Table 1).

Image analyses

We could reproducibly extract images of abnormally phosphorylated tau, and distinguish NFTs and other neuropil tau deposits (Figs. 1 and 2). Most NFT have large relative corresponding radii, most neuropil threads have small relative corresponding radii and small circularity, and grains have small relative corresponding radii and large circularity (Fig. 2E). However, it was difficult to discriminate precisely between neuropil threads and grains using our image analysis system, so we examined these as neuropil tau deposits.

Comparison of tau deposits between group A and group B

The relationship between the total area of tau pathology and the age at death is shown in Figure 3A. The total area of tau pathology in both groups A and B gradually increased from around 70 years of age (Fig. 3A). The total area of tau pathology in group B was significantly higher ($p < 0.001$) than that in group A (Fig. 3B). The area of NFT and neuropil tau deposits was also significantly higher ($p < 0.001$) in group B than in group A (Fig. 3C and D).

To examine the results in further detail, we subdivided groups A and B into 5-year age groups

according to their age at death (Supplementary Fig. 1 and Supplementary Table 1). Overall, the total area of hippocampal tau pathology increased with age, and the increase in tau pathology in older people in group B was substantially more than in group A. Some cases in group B had earlier deposits of abnormal tau, in their mid-60s (Fig. 3A).

When the group A data were analyzed by sex, the total area of tau pathology, NFT, and neuropil tau deposits of females was significantly higher ($p < 0.001$) than that of males (Table 3 and Supplementary Fig. 2). In group B, the total area of tau pathology and neuropil tau deposits in females were also significantly increased ($p = 0.035$ and 0.018, respectively). Although the mean and median areas of NFT in females were higher (Table 3 and Supplementary Fig. 2), these were not significant.

Levels of tau deposits relate to CERAD scores

To evaluate the relationship between tau deposits and CERAD stage, we categorized the data according to CERAD score and examined the total tau, NFT, and neuropil areas (Fig. 4, Table 4, and Supplementary Fig. 3). In the low CERAD score group, the total area of tau pathology was significantly larger ($p < 0.001$) in group B. In the high CERAD group, a similar trend was also observed ($p < 0.001$).

Levels of tau deposits relate to AD pathologic changes

We subdivided all cases into four levels of AD neuropathologic change; “Not”, “Low”, “Intermediate”, or “High” according to NIA-AA criteria, and then assessed the total tau area in each level (Table 5). The area of total tau was significantly increased in every level in group B (Fig. 5, and Supplementary Fig. 4).

Levels of tau deposits relate to DLB

We examined the influence of other neurodegenerative disorders, particularly DLB, as the pathology of DLB is known to frequently co-exist with AD pathology [17, 21].

To analyze the association between DLB and tau deposits, we subdivided the cases into 4 groups; (1) controls with no AD or DLB, (2) pure AD, (3) comorbid AD and DLB, and (4) pure DLB (Fig. 6A and B). Both the pure AD cases and the comorbid AD and DLB cases had greater areas of total tau pathology compared with the no AD or DLB controls or the pure DLB cases. We compared groups A and B, and found that the total tau area in pure AD was increased in group B (Fig. 7A), but not in DLB irrespective of the presence or absence of comorbid AD pathology (Fig. 7B and C).

DISCUSSION

In this study, we developed automated MATLAB morphometric analyses for the quantitative evaluation of abnormal tau deposits. Using this method, we examined the trend of tauopathies in the hippocampi from a series of autopsied cases of Hisayama. Total tau pathology, NFT, and neuropil tau deposits were significantly greater in the more recent group of subjects (group B). This is the first report of a recent trend of increased tauopathy in the hippocampi of Japanese elderly.

In agreement with our results, a recent autopsy study in the town of Hisayama revealed a significant increasing trend in the prevalence of AD and senile dementia of the NFT type (SD-NFT) [22]. Aging is considered one of the most important risk factors for accelerating tau pathology. The mean age at death was higher in group B than in group A, and associated with an increase in the area of total tau pathology. When comparing by age at death, the total area of tau pathology tended to increase in the aged brains of group B. Moreover, in the low and intermediate AD neuropathologic change groups, the gap in the mean age at death between groups A and B was small despite the obvious increases in tau deposits in group B. These results suggest that in recent years there may have been an emergence of risk factors for tau pathology

other than aging.

It has also been reported that the dominant cause of dementia in males in Hisayama has changed from vascular dementia (around 2005) to AD in 2016 [22]. In the present study, the time periods of sampling group A and group B were across this turning point, with group A being before 2005, and group B after. Our results reflect a changing trend in the type of dementia in this population. When analyzed by sex, the total areas of tau pathology, NFT, and neuropil tau deposits of females in group A were significantly higher than those of the males. In group B, the total area of tau pathology of females was significantly higher, while the difference in the area of NFT between males and females was not significant. This indicates that the level of tau pathology in males is approaching that of females. The Framingham study demonstrated that a non-demented 65-year-old male has a 6.3%, and a 65-year-old woman a 12%, chance of AD onset [23]. This gender difference in lifetime risk is thought to reflect the longevity of women. The increasing longevity of men in Japan may result in a notable increase in tauopathy: As society becomes more aged, more males will develop AD.

It is believed that abnormal tau phosphorylation is involved mainly in two processes, an amyloid-based process contributing to neocortical tangles [24] and an aging process that accounts for medial temporal lobe tangles. The amyloid-based process is widely described as

the amyloid cascade hypothesis [25-27]. Aging-related pathology can occur in the absence of significant Aβ plaque pathology and is largely restricted to the medial temporal lobe. This was previously called tangle-predominant senile dementia [28], or SD-NFT [29]. Recently, to describe a tau-related pathology that is commonly observed in the brains of older individuals, the term primary age-related tauopathy (PART) has been proposed [30]. PART can be distinguished from AD by the absence or scarcity of neuritic plaques and a Braak and Braak stage that is usually III or lower. Currently, tau pathology independent of the amyloid cascade has received wide attention. In our study, the area of tau deposits in group B was significantly increased in the group with low CERAD scores. This result suggests that the burdens of tau pathology are increasing in both men and women, partly independent of the amyloid cascade.

Recently, digital pathology and image analysis have been used to detail the characteristics and perform quantitative assessments of the neuropathological changes in neurodegenerative disorders [31-37]. Here, we developed new image-analysis programs in MATLAB for the quantitative evaluation of abnormal tau deposits. In particular, NFTs were extracted accurately and the total NFT numbers and areas were successfully obtained.

In a previous report, Savva et al. [38] demonstrated in a population-based cohort study the effect of age on the relationship between the classic neuropathological features of dementia and the

clinical manifestation of dementia. In their report, tangles gradually increased from the age of 70 years in non-demented patients. Our results are compatible with previous quantitative analyses of tauopathies, suggesting that the programs we developed are effective for quantifying tau. We performed quantitative analyses of not only NFTs but also neuropil deposits. Our results also revealed that neuropil tau and NFTs in area CA1 appear from around the age of 65 years.

In comorbid AD and DLB cases, α-synuclein pathology correlates with Aβ pathology, and tau tends to co-localize with α-synuclein in limbic areas [39, 40]. In this study, the total area of tau pathology in comorbid AD and DLB cases was slightly different to that in pure AD cases, and was higher than in non-AD and pure DLB cases. This may imply that the presence of DLB has a minor influence on the area of tau pathology. When comparing between groups A and B, only the pure AD cases in group B had greater areas of tau pathology. The comorbid AD and DLB cases had little difference in the area of tau pathology between groups A and B. This could be due to the relatively small number of comorbid AD and DLB cases and the difference in sex ratio in each group: no male and seven females in group A, and three males and three females in group B. This study has shown that the area of tau pathology in males tends to be lower than that in females. Thus, it should be noted that the areas of total tau pathology could be affected

by the difference in the sex ratios between the groups.

One of the limitations of this study is that all participants were residents of Hisayama town, Japan, and therefore may not reflect other populations and races. Recently, some European population-based studies showed the incidence of dementia was declining in older people [41, 42]. On the other hand, in China [43] and some other Asian countries the number of people with dementia continues to increase. *The World Alzheimer Report 2015* [1] suggested that regional trends of dementia prevalence fall into three broad groups: Developed regions have a high baseline of dementia cases and a mild increase, Latin America and Africa have increasing numbers of people with dementia, and Asian countries such as India and China have a high baseline and relatively rapid increases in case numbers. Our results may fit with the general regional trend occurring in Asia.

CONCLUSION

In this study, we developed effective automated programs for the morphometric study of abnormally phosphorylated tau deposits. We then revealed that tau pathology gradually and steadily becomes more severe both in amyloid-dependent and aging-dependent processes, particularly in older Japanese people.

Aging could be one of the crucial backgrounds to increasing burdens of tau pathology. However, we revealed that even in low CERAD score cases increases in tau pathology occurred, suggesting that there are other risk factors for the development of tau pathology. Further studies are needed to research these risk factors in greater detail.

ACKNOWLEDGMENTS

This research was funded by JSPS KAKENHI Grant Number 26290017 and by the Japan Agency for Medical Research and development, AMED Grant Number 15dk0207003h0003.

The authors thank Ms. Yumi Hamamoto for her technical assistance. We have no conflicts of interest to disclose.

REFERENCES

[1] Martin Prince AW, Maelenn Guerchet, Gemma-Claire Ali, Yu-Tzu Wu, Prina M (2015.) World Alzheimer report 2015 the global impact of dementia: Alzheimer's Disease International. *London,* .

[2] Matsuzaki T, Sasaki K, Hata J, Hirakawa Y, Fujimi K, Ninomiya T, Suzuki SO, Kanba S, Kiyohara Y, Iwaki T (2011) Association of Alzheimer disease pathology with abnormal lipid metabolism: the Hisayama study. *Neurology* **77**, 1068–1075.

[3] Matsuzaki T, Sasaki K, Tanizaki Y, Hata J, Fujimi K, Matsui Y, Sekita A, Suzuki SO, Kanba S, Kiyohara Y, Iwaki T (2010) Insulin resistance is

associated with the pathology of Alzheimer disease: the Hisayama study. *Neurology* **75**, 764–770.

[4] Kubo M, Hata J, Doi Y, Tanizaki Y, Iida M, Kiyohara Y (2008) Secular trends in the incidence of and risk factors for ischemic stroke and its subtypes in Japanese community: the Hisayama study. *Acta Psychiatr Scand* **122**, 319–325.

[5] Sekita A, Ninomiya T, Tanizaki Y, Doi Y, Hata J, Yonemoto K, Arima H, Sasaki K, Iida M, Iwaki T, Kanba S, Kiyohara Y (2010) Trends in prevalence of Alzheimer's disease and vascular dementia in a Japanese community: the Hisayama Study. *Acta Psychiatr Scand* **122**, 319–325.

[6] Kishimoto H, Ohara T, Hata J, Ninomiya T, Yoshida D, Mukai N, Nagata M, Ikeda F, Fukuhara M, Kumagai S, Kanba S, Kitazono T, Kiyohara Y (2016) The long-term association between physical activity and risk of dementia in the community: the Hisayama study. *Eur J Epidemiol* **31**, 267–274.

[7] Ohara T, Ninomiya T, Hata J, Ozawa M, Yoshida D, Mukai N, Nagata M, Iwaki T, Kitazono T, Kanba S, Kiyohara Y (2015) Midlife and late-life smoking and risk of dementia in the community: The Hisayama study. *J Am Geriatr Soc* **63**, 2332–2339.

[8] Ozawa M, Ninomiya T, Ohara T, Doi Y, Uchida K, Shirota T, Yonemoto K, Kitazono T, Kiyohara Y (2013) Dietary patterns and risk of dementia in an elderly Japanese population: the Hisayama study. *Am J Clin Nutr* **97**, 1076–1082.

[9] Association. AP (1987) Diagnostic and statistical manual of mental disorders. 3rd ed, revised. *Washington, DC: American Psychiatric Association.*

[10] Braak H, Braak E (1991) Demonstration of amyloid deposits and neurofibrillary changes in whole brain sections. *Brain Pathology* **1**, 213–216.

[11] Mirra SS, Heyman A, McKeel D, Sumi SM, Crain BJ, Brownlee LM, Vogel FS, Hughes JP, van Belle G, Berg L (1991) The Consortium to Establish a Registry for Alzheimer's Disease (CERAD). Part II. Standardization of the neuropathologic assessment of Alzheimer's disease. *Neurology* **41**, 479–486.

[12] Braak H, Braak E (1991) Neuropathological stageing of Alzheimer-related changes. *Acta Neuropathol* **82**, 239–259.

[13] Braak H, Braak E (1997) Diagnostic criteria for neuropathologic assessment of Alzheimer's disease. *Neurobiol Aging* **18**, S85–88.

[14] (1997) Consensus recommendations for the postmortem diagnosis of Alzheimer's disease. The National Institute on Aging, and Reagan Institute working group on diagnostic criteria for the neuropathological assessment of Alzheimer's disease. *Neurobiol Aging* **18**, S1–2.

[15] Hyman BT, Phelps CH, Beach TG, Bigio EH, Cairns NJ, Carrillo MC, Dickson DW, Duyckaerts C, Frosch MP, Masliah E, Mirra SS, Nelson PT, Schneider JA, Thal DR, Thies B, Trojanowski JQ, Vinters HV, Montine TJ (2012) National Institute on Aging-Alzheimer's Association guidelines for the neuropathologic assessment of Alzheimer's disease. *Alzheimers Dement* **8**, 1–13.

[16] McKeith IG, Dickson DW, Lowe J, Emre M, O'Brien JT, Feldman H, Cummings J, Duda JE, Lippa C, Perry EK, Aarsland D, Arai H, Ballard CG, Boeve B, Burn DJ, Costa D, Del Ser T, Dubois B, Galasko D, Gauthier S, Goetz CG, Gomez-Tortosa E, Halliday G, Hansen LA, Hardy J, Iwatsubo T, Kalaria RN, Kaufer D, Kenny RA, Korczyn A, Kosaka K, Lee VM, Lees A, Litvan I, Londos E, Lopez OL, Minoshima S, Mizuno Y, Molina JA, Mukaetova-Ladinska EB, Pasquier F, Perry RH, Schulz JB, Trojanowski JQ, Yamada M, Consortium on DLB (2005) diagnosis and management of dementia with Lewy bodies: third report of the DLB Consortium. *Neurology* **65**, 1863–1872.

[17] Fujimi K, Sasaki K, Noda K, Wakisaka Y, Tanizaki Y, Matsui Y, Sekita A, Iida M, Kiyohara Y, Kanba S, Iwaki T (2008) Clinicopathological outline of dementia with Lewy bodies applying the revised criteria: the Hisayama study. *Brain Pathol* **18**, 317–325.

[18] Jain AK (1989) Fundamentals of digital image processing. *New Jersey, United States of America: Prentice Hall.*, pp. 68, 71, 73.

[19] MathWorks Inc, http://jp.mathworks.com/help/images/ref/rgb2lab.html?lang=en, Accessed on August 4, 2016.

[20] MacQueen J (1967) in *Proceedings of the Fifth Berkeley Symposium on Mathematical Statistics and Probability, Volume 1: Statistics* University of

California Press, Berkeley, Calif, 281–297.

[21] Pletnikova O, West N, Lee MK, Rudow GL, Skolasky RL, Dawson TM, Marsh L, Troncoso JC (2005) Abeta deposition is associated with enhanced cortical alpha-synuclein lesions in Lewy body diseases. *Neurobiol Aging* **26**, 1183–1192.

[22] Honda H, Sasaki K, Hamasaki H, Shijo M, Koyama S, Ohara T, Ninomiya T, Kiyohara Y, Suzuki SO, Iwaki T (2016) Trends in autopsy-verified dementia prevalence over 29 years of the Hisayama study. *Neuropathology*.

[23] Seshadri S, Wolf PA, Beiser A, Au R, McNulty K, White R, D'Agostino RB (1997) Lifetime risk of dementia and Alzheimer's disease. The impact of mortality on risk estimates in the Framingham Study. *Neurology* **49**, 1498–1504.

[24] Mungas D, Tractenberg R, Schneider JA, Crane PK, Bennett DA (2014) A 2-process model for neuropathology of Alzheimer's disease. *Neurobiol Aging* **35**, 301–308.

[25] Hardy JA, Higgins GA (1992) Alzheimer's disease: the amyloid cascade hypothesis. *Science* **256**, 184–185.

[26] Hardy J, Allsop D (1991) Amyloid deposition as the central event in the aetiology of Alzheimer's disease. *Trends Pharmacol Sci* **12**, 383–388.

[27] Evin G, Weidemann A (2002) Biogenesis and metabolism of Alzheimer's disease Abeta amyloid peptides. *Peptides* **23**, 1285–1297.

[28] Jellinger KA, Bancher C (1998) Senile dementia with tangles (tangle predominant form of senile dementia). *Brain Pathol* **8**, 367–376.

[29] Yamada M, Itoh Y, Sodeyama N, Suematsu N, Otomo E, Matsushita M, Mizusawa H (2001) Senile dementia of the neurofibrillary tangle type: a comparison with Alzheimer's disease. *Dement Geriatr Cogn Disord* **12**, 117–126.

[30] Crary JF, Trojanowski JQ, Schneider JA, Abisambra JF, Abner EL, Alafuzoff I, Arnold SE, Attems J, Beach TG, Bigio EH, Cairns NJ, Dickson DW, Gearing M, Grinberg LT, Hof PR, Hyman BT, Jellinger K, Jicha GA, Kovacs GG, Knopman DS, Kofler J, Kukull WA, Mackenzie IR, Masliah E, McKee A, Montine TJ, Murray ME, Neltner JH, Santa-Maria I, Seeley WW, Serrano-Pozo A, Shelanski ML, Stein T, Takao M, Thal DR, Toledo JB,

Troncoso JC, Vonsattel JP, White CL, 3rd, Wisniewski T, Woltjer RL, Yamada M, Nelson PT (2014) Primary age-related tauopathy (PART): a common pathology associated with human aging. *Acta Neuropathol* **128**, 755–766.

[31] Chibnik LB, Shulman JM, Leurgans SE, Schneider JA, Wilson RS, Tran D, Aubin C, Buchman AS, Heward CB, Myers AJ, Hardy JA, Huentelman MJ, Corneveaux JJ, Reiman EM, Evans DA, Bennett DA, De Jager PL (2011) CR1 is associated with amyloid plaque burden and age-related cognitive decline. *Ann Neurol* **69**, 560–569.

[32] Dunn WD, Jr., Gearing M, Park Y, Zhang L, Hanfelt J, Glass JD, Gutman DA (2015) Applicability of digital analysis and imaging technology in neuropathology assessment. *Neuropathology*.

[33] Murray ME, Graff-Radford NR, Ross OA, Petersen RC, Duara R, Dickson DW (2011) Neuropathologically defined subtypes of Alzheimer's disease with distinct clinical characteristics: a retrospective study. *Lancet Neurol* **10**, 785–796.

[34] Robinson JL, Geser F, Corrada MM, Berlau DJ, Arnold SE, Lee VM, Kawas CH, Trojanowski JQ (2011) Neocortical and hippocampal amyloid-beta and tau measures associate with dementia in the oldest-old. *Brain* **134**, 3708–3715.

[35] Whitwell JL, Dickson DW, Murray ME, Weigand SD, Tosakulwong N, Senjem ML, Knopman DS, Boeve BF, Parisi JE, Petersen RC, Jack CR, Jr., Josephs KA (2012) Neuroimaging correlates of pathologically defined subtypes of Alzheimer's disease: a case-control study. *Lancet Neurol* **11**, 868–877.

[36] Armstrong RA, Cairns NJ (2009) Size frequency distribution of the beta-amyloid (abeta) deposits in dementia with Lewy bodies with associated Alzheimer's disease pathology. *Neurol Sci* **30**, 471–477.

[37] Noda K, Sasaki K, Fujimi K, Wakisaka Y, Tanizaki Y, Wakugawa Y, Kiyohara Y, Iida M, Aizawa H, Iwaki T (2006) Quantitative analysis of neurofibrillary pathology in a general population to reappraise neuropathological criteria for senile dementia of the neurofibrillary tangle type (tangle-only dementia): the Hisayama study. *Neuropathology* **26**, 508–

518.

[38] Savva GM, Wharton SB, Ince PG, Forster G, Matthews FE, Brayne C (2009) Age, neuropathology, and dementia. *New England Journal of Medicine* **360**, 2302–2309.

[39] Marsh SE, Blurton-Jones M (2012) Examining the mechanisms that link beta-amyloid and alpha-synuclein pathologies. *Alzheimers Res Ther* **4**, 11.

[40] Colom-Cadena M, Gelpi E, Charif S, Belbin O, Blesa R, Marti MJ, Clarimon J, Lleo A (2013) Confluence of alpha-synuclein, tau, and beta-amyloid pathologies in dementia with Lewy bodies. *J Neuropathol Exp Neurol* **72**, 1203–1212.

[41] Satizabal CL, Beiser AS, Chouraki V, Chene G, Dufouil C, Seshadri S (2016) Incidence of dementia over three decades in the Framingham heart study. *N Engl J Med* **374**, 523–532.

[42] Matthews FE, Stephan BC, Robinson L, Jagger C, Barnes LE, Arthur A, Brayne C (2016) A two decade dementia incidence comparison from the cognitive function and ageing studies I and II. *Nat Commun* **7**, 11398.

[43] Chen R, Hu Z, Wei L, Ma Y, Liu Z, Copeland JR (2011) Incident dementia in a defined older Chinese population. *PLoS One* **6**, e24817.

Table 1

Profiles of analyzed cases

	1998–2003	2009–2014	*p* value
Total cases (mean age ± SD)	203 (78.8 ± 12.8)	232 (83.0 ± 10.8)	< 0.001
Male	108 (74.0 ± 12.4)	120 (80.4 ± 10.3)	< 0.001
Female	95 (84.2 ± 11.0)	112 (85.8 ± 10.6)	0.286
AD cases (mean age ± SD)			
Total	34 (87.4 ± 6.84)	71 (90.3 ± 6.16)	0.035
Male	7 (84.7 ± 8.0)	27 (88.3 ± 6. 66)	0.302
Female	27 (88.0 ± 6.5)	44 (91.5 ± 5.57)	0.028
CERAD cases (mean age ± SD)			
None	71 (71.4 ± 14.6)	48 (75.5 ± 10.2)	0.075
Sparse	32 (79.8 ± 11.0)	49 (83.1 ± 11.4)	0.202
Moderate	31 (82.2 ± 10.6)	27 (79.9 ± 11.9)	0.451
Frequent	69 (84.3 ± 8.32)	108 (87.1 ± 8.31)	0.033
Braak and Braak stage cases (mean age ± SD)			
0–II	71 (70.2 ± 14.6)	55 (72.4 ± 11.4)	0.352
III, IV	81 (82.3 ± 9.08)	73 (83.0 ± 8.52)	0.667
V, VI	51 (85.0 ± 8.60)	104 (88.7 ± 7.09)	0.009

AD, Alzheimer’s disease; CERAD, Consortium to Establish a Registry for Alzheimer's disease; SD, standard deviation.

Table 2.

Pathological diagnoses of the patients.

	1998–2003		2009–2014	
Diagnosis	Male cases/ female cases	mean age at death ± SD	Male cases/ female cases	mean age at death ± SD
Not demented	90/51	75.2 ± 13.3	76/50	78.1 ± 11.1
AD	3/13	87.4 ± 6.6	19/36	91.4 ± 5.6
AD+AGD	-	-	1/0	81
AD+DLB	0/6	86.4 ± 6.5	3/3	89.7 ± 3.3
AD+DLB+VD	0/1	93	-	-
AD+PD with dementia	-	-	1/0	88
AD+PSP	1/0	89	-	-
AD+VD	1/4	88.8 ± 7.2	2/5	86.3 ± 7.2
sCJD+AD	-	-	1/0	73
DLB	1/4	86.6 ± 4.9	2/1	85.7 ± 4.04
AGD	-	-	0/1	94
PD with Dementia	-	-	1/0	64
SD-NFT	1/1	90.5 ± 2.1	5/4	88.9 ± 2.2
SD-NFT+DLB+VD	1/0	95	-	-
SD-NFT+AGD	-	-	1/2	91.7 ± 6.4
PSP	-	-	1/0	75
VD	9/7	84.1 ± 6.4	3/7	84.3 ± 6.6
VD+DLB	3/0	92.7 ± 6.5	-	-
VD+SD-NFT	-	-	2/2	89.5 ± 6.2
Other dementia	1/0	81	2/1	80.7 ± 4.7
Total	203		232	

AD, Alzheimer’s disease; DLB, dementia with Lewy bodies; SD-NFT, senile dementia of neurofibrillary tangle type; VD, vascular dementia; AGD, argyrophilic grain disease; PD, Parkinson’s disease; sCJD, sporadic Creutzfeldt-Jakob disease; PSP, progressive supranuclear palsy; and Other dementia: Pick disease (*n* = 1), lymphoma (*n* = 1), normal pressure hydrocephalus (*n* = 1), mitochondrial encephalomyopathy (*n* = 1). The “Not demented” group consisted of participants with no neurological deficits (*n* = 121), cerebral vascular disease (*n* =

124), head trauma (*n* = 15), brain metastases (*n* = 9), meningitis (*n* = 1), meningioma (*n* = 1), and primary central nervous system lymphoma (*n* = 2).

Table 3

Examination of the total areas of tau pathology, NFTs, and neuropil tau deposits divided by gender in group A and group B.

	male median (min–max)	Female median (min–max)	*p* value
Group A (1998–2003)			
Total area (%)	0.204 (0–3.45)	0.615 (0–6.46)	< 0.001
NFT (%)	0.155 (0–2.46)	0.507 (0–4.11)	< 0.001
Neuropil tau deposits (%)	0.036 (0–1.43)	0.135 (0–2.34)	< 0.001
Group B (2009–2014)			
Total area (%)	0.873 (0–8.77)	1.510 (0–7.37)	0.035
NFT (%)	0.626 (0–4.64)	0.931 (0–4.70)	0.190
Neuropil tau deposits (%)	0.257 (0–4.83)	0.427 (0–4.05)	0.018

Table 4

Examination of the total area of tau pathology according to CERAD staging.

	1998–2003	2009–2014	*p* value
CERAD: None and Sparse (n)	103	97	
mean age ± SD	74.0 ± 14.1	79.3 ± 11.4	0.004
tauopathy: median (min–max)	0.168 (0–3.621)	0.648 (0–4.680)	0.001
CERAD: Moderate and Frequent (n)	100	135	
mean age ± SD	83.7 ± 9.1	85.7 ± 9.5	0.107
tauopathy: median (min–max)	0.879 (0–6.456)	1.167 (0–8.771)	< 0.001

Table 5

Profiles of cases according to AD neuropathologic changes

	1998–2003		2009–2014	
AD neuropathologic change	Male cases/ female cases	mean age at death ± SD	Male cases/ female cases	mean age at death ± SD
Not	40/31	71.4 ± 14.6	26/22	75.5 ± 10.2
Low	32/20	79.3 ± 10.5	37/28	80.4 ± 12.3
Intermediate	24/16	84.3 ± 8.9	23/22	85.0 ± 8.2
High	12/28	85.7 ± 8.0	34/40	89.0 ± 6.9
Total	203		232	

Supplementary Table 1

Examination of the total area of tau pathology comparing 1998–2003 and 2009–2014 with groups A and B subdivided into 5-year age groups

age		1998–2003	2009–2014
< 64	(n)	28	16
	mean age ± SD	54.4 ± 8.2	57.6 ± 6.1
	median of total tau (min–max)	0 (0–0.27)	0 (0–0.52)
65–69	(n)	9	12
	mean age	66.6 ± 1.5	67.2 ± 1.7
	median of total tau (min–max)	0 (0–2.66)	0.22 (0–3.48)
70–74	(n)	24	15
	mean age	71.9 ± 1.3	82.1 ± 1.3
	median of total tau (min–max)	0.11 (0–2.61)	0.31 (0–3.44)
75–79	(n)	34	27
	mean age ± SD	77.4 ± 1.5	77.0 ± 1.4
	median of total tau (min–max)	0.39 (0–6.46)	0.62 (0–4.10)
80–84	(n)	33	42
	mean age	82.1 ± 1.3	82.1 ± 1.5
	median of total tau (min–max)	0.55 (0–3.60)	0.86 (0.03–7.37)
85–89	(n)	33	56
	mean age	87.2 ± 1.4	87.1 ± 1.5
	median of total tau (min–max)	0.62 (0–3.83)	1.62 (0.05–6.28)
90–94	(n)	29	42
	mean age ± SD	91.9 ± 1.6	92.1 ± 1.9
	median of total tau (min–max)	1.01 (0–4.06)	2.03 (0.15–6.28)
95–99	(n)	12	14

	mean age	96.7 ± 1.7	96.4 ± 1.5
	median of total tau (min–max)	1.08 (0.21–3.07)	2.64 (0.20–6.51)
< 100	(n)	1	9
	mean age	100	100.1 ± 1.6
	median of total tau (min–max)	1.17	2.14 (1.16–0.67)

FIGURE LEGENDS

Fig. 1. Workflow for the image analysis.

Fig. 2. Detail analyzed image.

A: The area of hippocampal CA1 immunostained using anti-hyperphosphorylated tau antibody is captured using 20× objective lens with a total field size of 704 × 528 mm^2. B: Abnormal tau deposits are extracted. C, D: Higher magnifications of squared areas in panel A and B, respectively. NFT is marked with *, and neuropil threads are pointed out with arrows in panels C and D. E: The extracted image is classified depend on their relative corresponding radius (x-axis) and circularity (y-axis). A scatter plot of the circularity versus the relative corresponding radius was constructed to classify abnormal tau deposits.

Fig. 3. Comparison of the total area of tau pathology, NFTs, and neuropil tau deposits between groups A and B.

A, C, D: Total areas of tau pathology (A), NFTs (C), and neuropil tau deposits (D) according to age at death are shown. Group A (1998–2003) and group B (2009–2014) are shown as circles and deltas, respectively. B: The area of total tau of group B is significantly higher than that of group A. *Mann–Whitney *U* test, $p < 0.001$.

Fig. 4. Plotting of the total area of tau pathology according to CERAD staging.

Group A (1998–2003) and group B (2009–2014) are shown as circles and deltas, respectively. The total area of tau pathology of group B is higher than that of group A irrespective of CERAD stage.

Fig. 5. Total area of tau pathology according to the levels of AD neuropathologic changes.

Group A (1998–2003) and group B (2009–2014) are shown as circles and deltas, respectively. The total areas of tau pathology in group B are significantly higher than those in group A in all levels of AD neuropathologic change.

Fig. 6. Total area of tau pathology according to AD and Dementia with Lewy bodies (DLB) pathology.

Black, yellow, red, and green circles show (1) non-AD and non-DLB (Non-AD/DLB) cases, (2) AD without DLB (Pure AD) cases, (3) comorbid AD and DLB (AD and DLB) cases, and (4) DLB without AD (pure DLB) cases, respectively.

A: Scatterplot and B: box plot of the total area of tau pathology showing AD and AD with DLB cases tend to have a greater total tau pathology area.

Fig. 7. Total area of tau pathology in groups A and B according to AD and DLB pathology.

A: The total tau pathology of AD without DLB (Pure AD) cases of group B is significantly higher compared with group A.

B, C: No significant differences are observed between groups A and B.

SUPPLEMENTARY FIGURE LEGENDS

Supplementary Fig. 1. Histogram of the median total tau pathology divided into 5-year age

groups**.**

The black and gray (with slanting line) histograms correspond to the medians of the areas of total tau pathology in groups A (1998–2003) and B (2009–2014), respectively. The median areas of total tau pathology in group B are always larger than those in group A.

Supplementary Fig. 2. Examination of the total areas of tau pathology, NFTs, and neuropil tau deposits divided by sex in group A (A, C, E) and group B (B, D, F).

The total areas of both tau pathology (A, B) and neuropil tau deposits (E, F) are significantly higher in females than in males in both groups. The area of NFTs in females in group A is significantly higher than that in males (C), but there is no significant difference between males and females in group B (D).

Supplementary Fig. 3. Examination of the total area of tau pathology according to CERAD staging.

A: CERAD: none and sparse. B: CERAD: moderate and frequent. Group A (1998–2003) and group B (2009–2014) are shown as circles and deltas, respectively. The total areas of tau pathology of group B are significantly higher than those of group A in both the lower and

higher CERAD stages.

Supplementary Fig. 4. Total area of tau pathology according to the level of AD neuropathologic change in group A (A, C, E, G) and group B (B, D, F, H)

The total area of tau pathology of group B tended to be higher than that of group A in all levels of AD neuropathologic changes.

Fig. 1

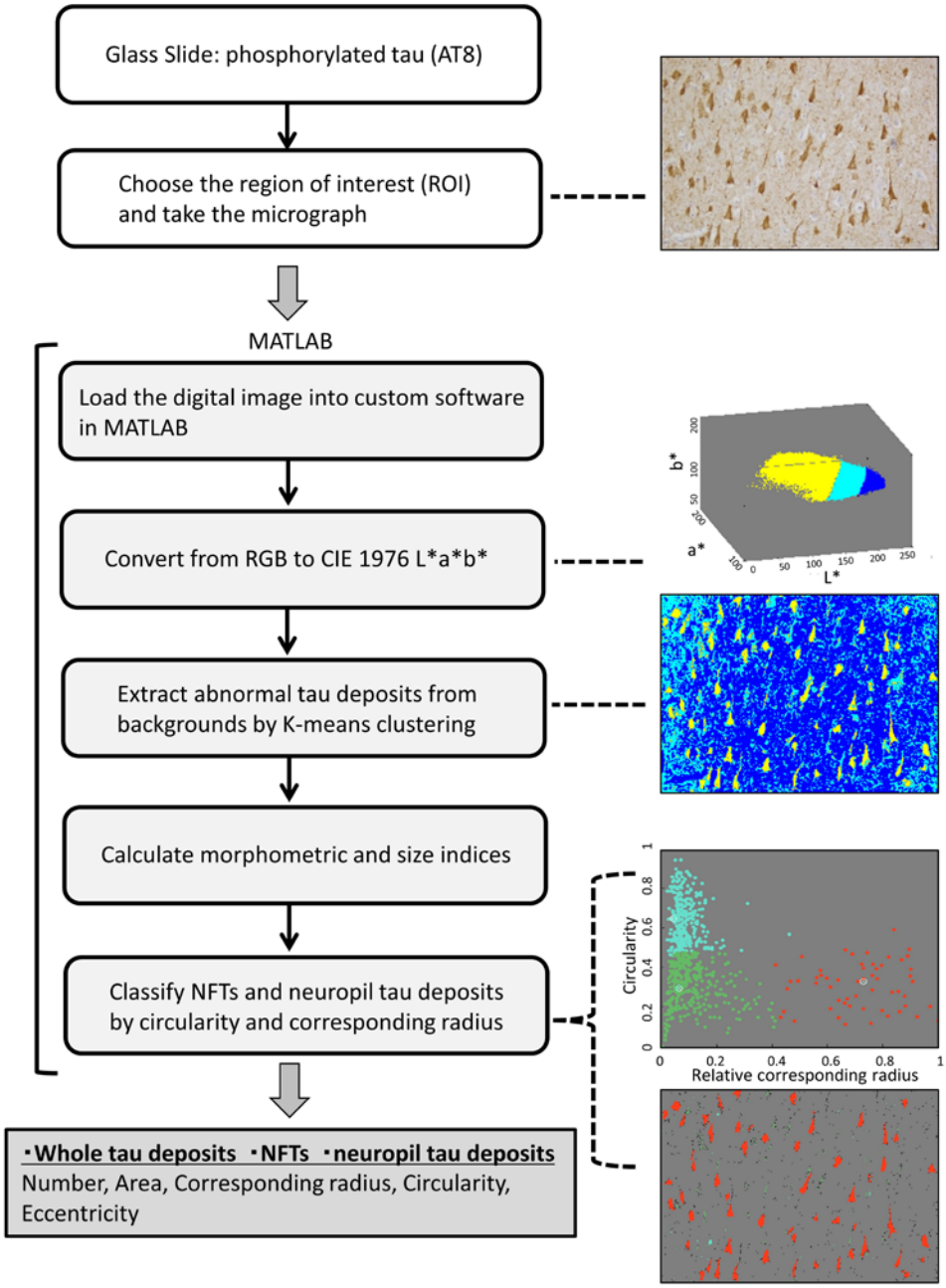
Glass Slide: phosphorylated tau (AT8)
Choose the region of interest (ROI) and take the micrograph
MATLAB
Load the digital image into custom software in MATLAB
Convert from RGB to CIE 1976 L*a*b*
Extract abnormal tau deposits from backgrounds by K-means clustering
Calculate morphometric and size indices
Classify NFTs and neuropil tau deposits by circularity and corresponding radius
・Whole tau deposits ・NFTs ・neuropil tau deposits
Number, Area, Corresponding radius, Circularity, Eccentricity
b*
a*
L*
Circularity
Relative corresponding radius

Fig. 2

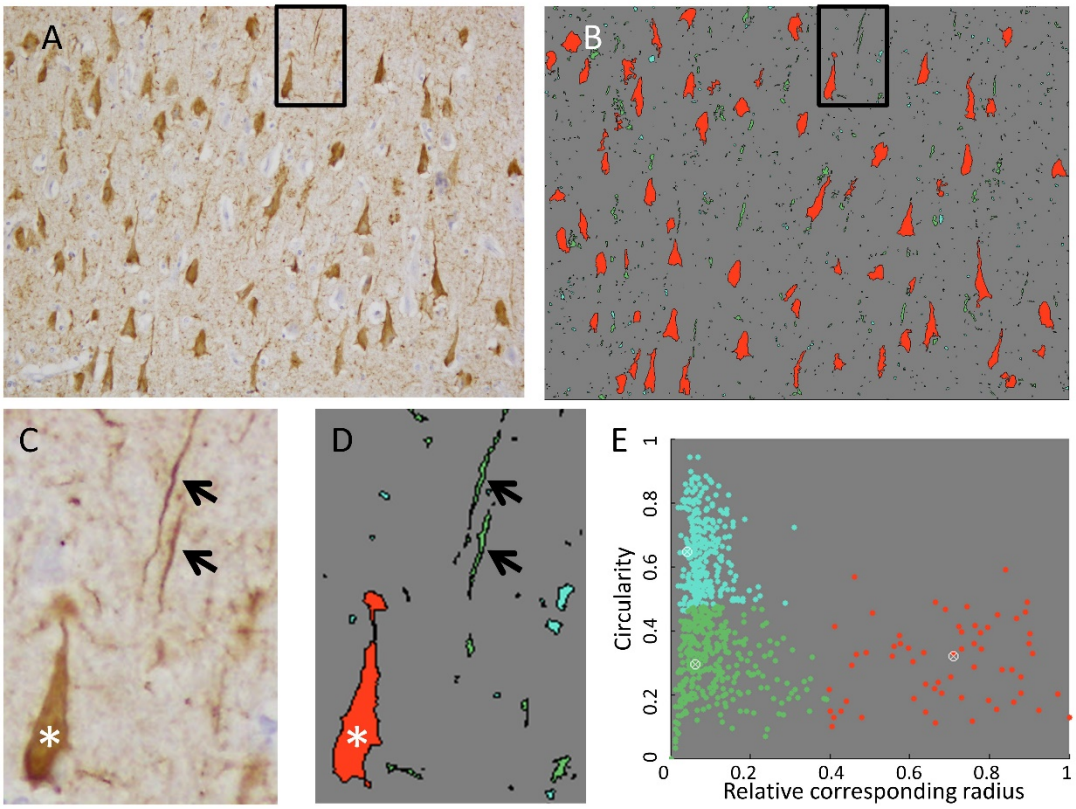
A
B
C
D
E
Circularity
Relative corresponding radius
0
0.2
0.4
0.6
0.8
1

Fig. 3

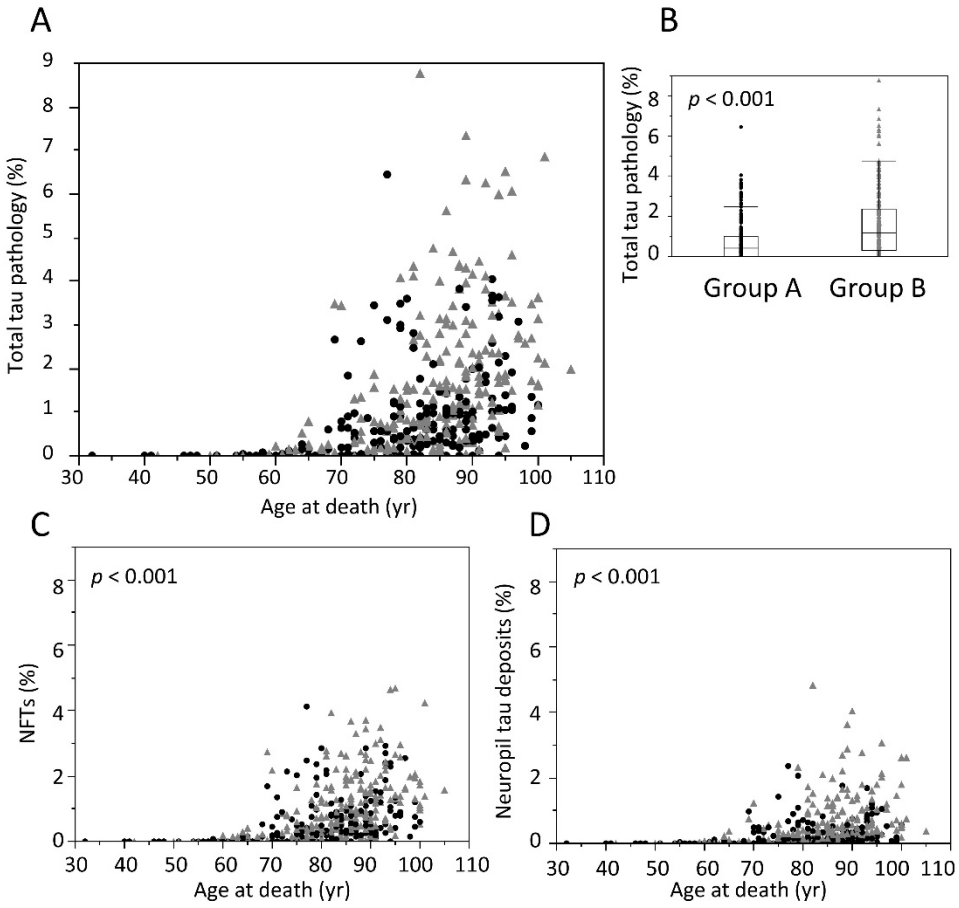
A
Total tau pathology (%)
Age at death (yr)
B
Total tau pathology (%)
p < 0.001
Group A
Group B
C
NFTs (%)
p < 0.001
Age at death (yr)
D
Neuropil tau deposits (%)
p < 0.001
Age at death (yr)

Fig. 4

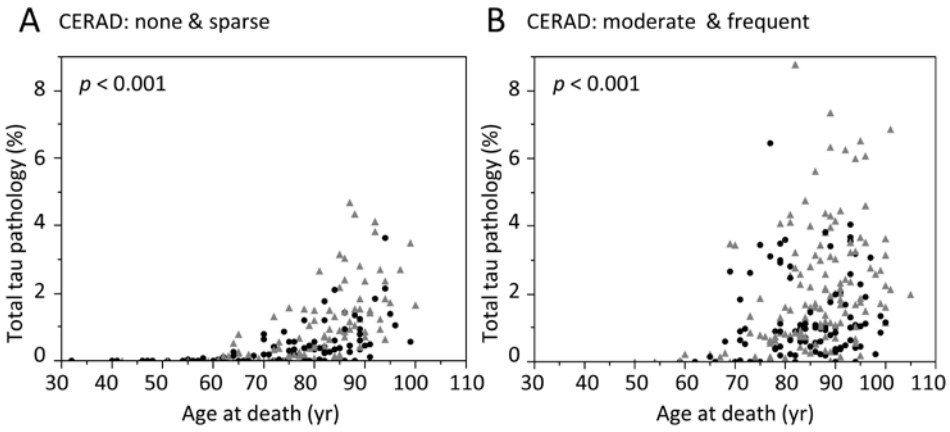
A CERAD: none & sparse
B CERAD: moderate & frequent
p < 0.001
p < 0.001
Total tau pathology (%)
Age at death (yr)
0
2
4
6
8
30
40
50
60
70
80
90
100
110

Fig. 5

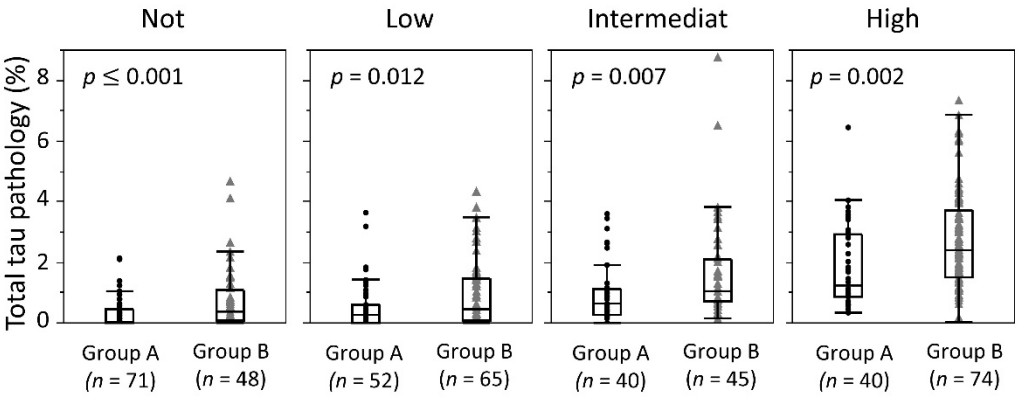
Not
Low
Intermediat
High
p ≤ 0.001
p = 0.012
p = 0.007
p = 0.002
Total tau pathology (%)
Group A (n = 71)
Group B (n = 48)
Group A (n = 52)
Group B (n = 65)
Group A (n = 40)
Group B (n = 45)
Group A (n = 40)
Group B (n = 74)

Fig. 6

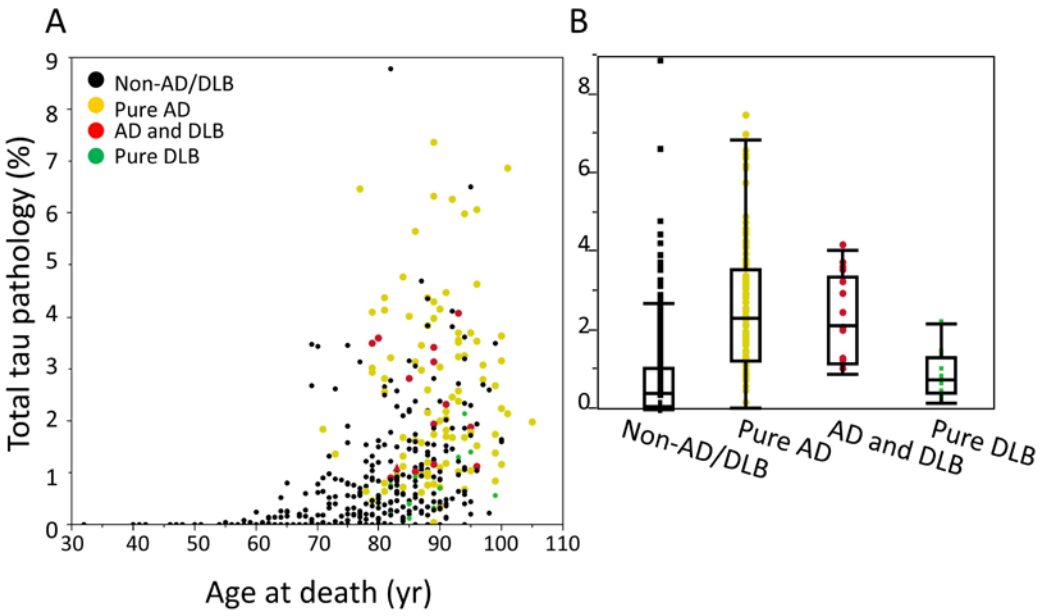
A
B
Non-AD/DLB
Pure AD
AD and DLB
Pure DLB
Total tau pathology (%)
Age at death (yr)
Non-AD/DLB
Pure AD
AD and DLB
Pure DLB

Fig. 7

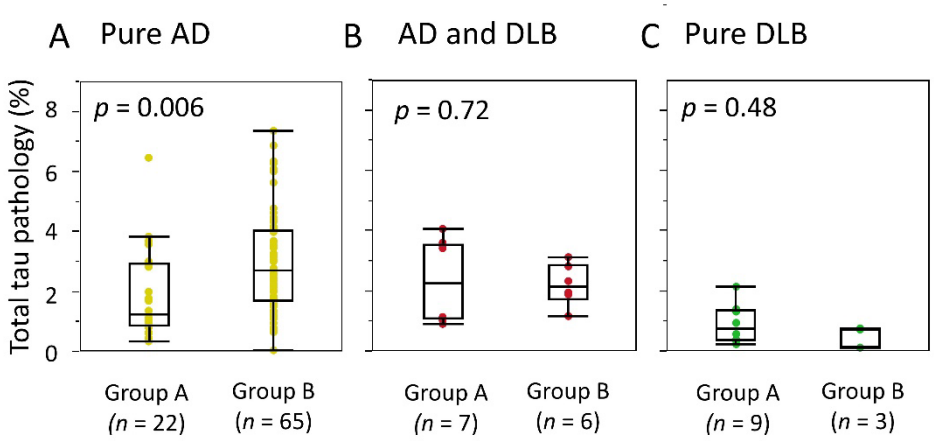
A Pure AD
B AD and DLB
C Pure DLB
Total tau pathology (%)
p = 0.006
p = 0.72
p = 0.48
Group A (n = 22)
Group B (n = 65)
Group A (n = 7)
Group B (n = 6)
Group A (n = 9)
Group B (n = 3)

Supplementary Fig. 1

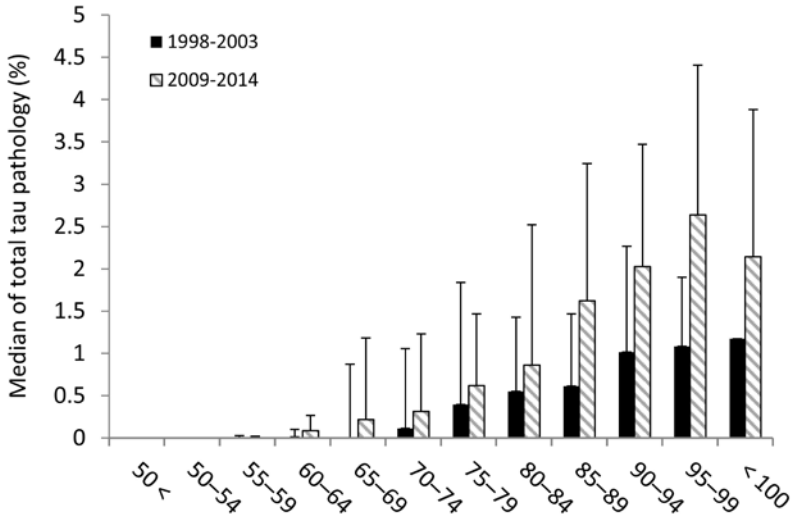

Supplementary Fig. 2

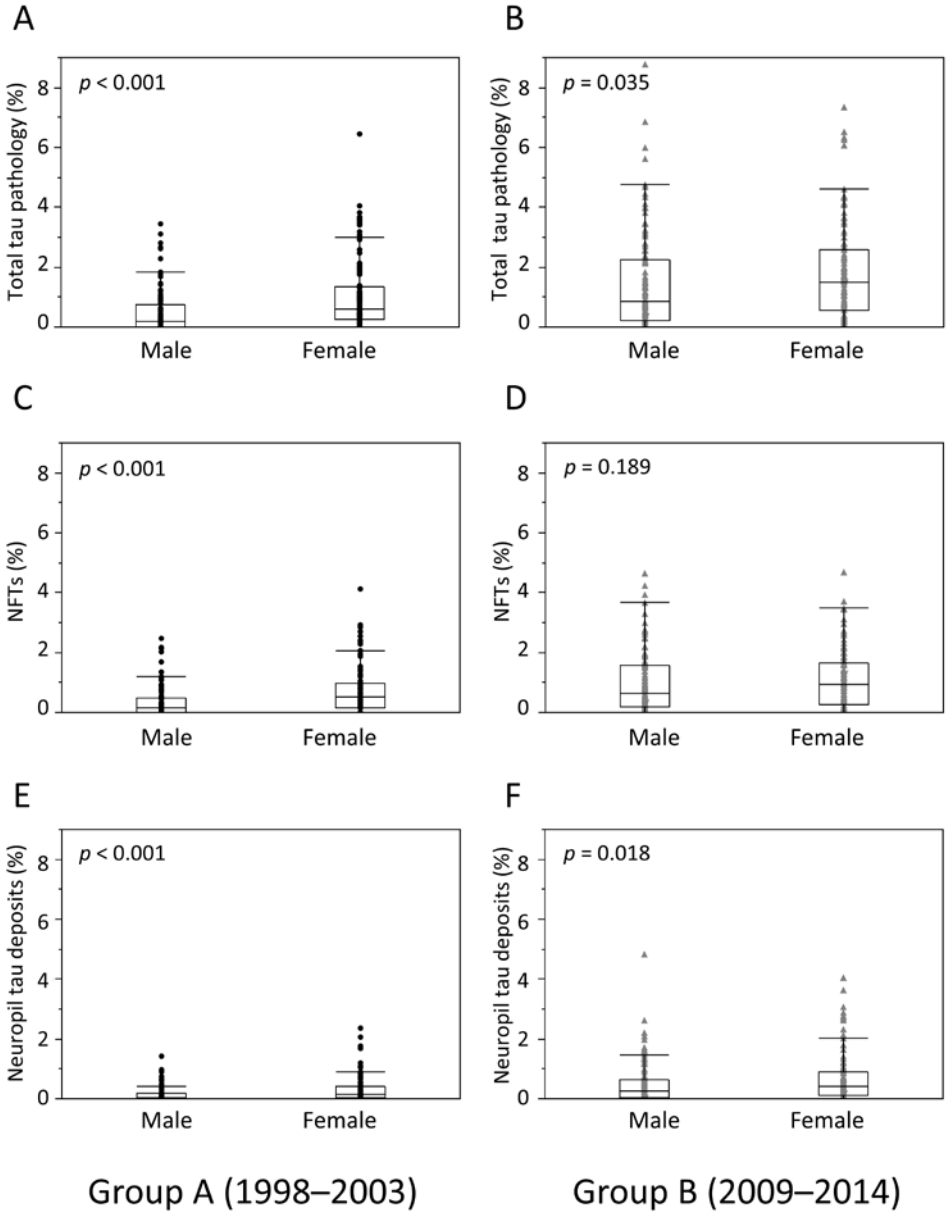

Supplementary Fig. 3

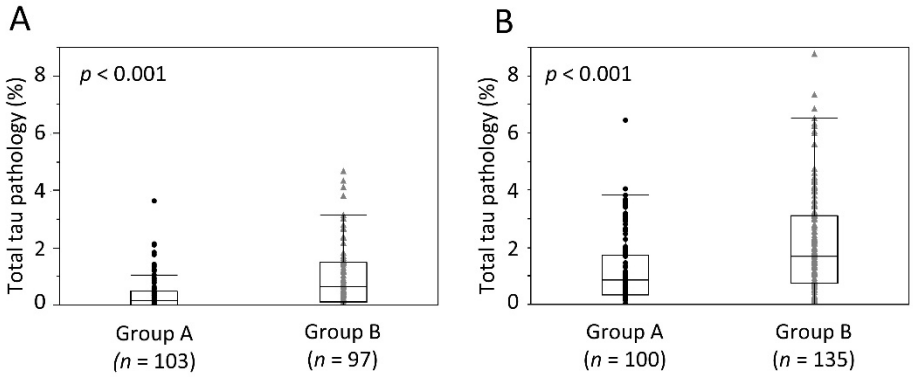

Supplementary Fig. 4